AIAA JOURNAL
Vol. 34, No. 9, September 1996

Coaxial Jets from Lobed-Mixer Nozzles

R. Ramesh Kumar* and Job Kurian†
Indian Institute of Technology, Madras 600 036, India

Experiments were conducted to study the jet dynamics of unconfined and confined coaxial high-speed flows from radially lobed nozzles. The shear-layer growth rate of the lobed nozzles was found to be considerably higher than that of a conical nozzle. Pressure profiles indicated increased radial uniformity and transport of properties between flows. Increases in lobe height and number of lobes were associated with enhanced mixing and larger total pressure drops. The thrust loss observed was due primarily to divergent nozzle flow and duct friction losses. Use of a confining duct forced interaction of the flows and enhanced mixing. Compression of the primary flow produced intense compression-expansion regions in the flowfield. Another advance over earlier studies is the visualization of the axial vortices generated by lobed nozzles. These vortices can be linked to the observed cross-plane transport of properties.

Nomenclature

D = diameter
D_P = total pressure drop parameter
l = length of mixing tube
M = Mach number
$\dot{m}$ = mass flow rate
P = total pressure
p = static pressure
R = radius
r = radial coordinate
T = thrust
u = velocity
x = axial coordinate
δ = shear-layer thickness
ρ = density
η = mixing parameter

Subscripts

c = convective
cl = centerline
e = equivalent
edge = edge of shear layer
ex = nozzle exit plane
P = primary stream
S = secondary stream

Introduction

EXTENSIVE experimental investigations in planar shear layers by Chinzei et al.,[1] Papamoschou and Roskho,[2] Goebel and Dutton,[3] Clemens and Mungal,[4] and others have revealed a considerable reduction in shear-layer growth rates with increase in compressibility. A similar trend for coaxial jets was observed by Schadow et al.,[5] Gutmark et al.,[6] Tillman et al.,[7] and others. The utility of supersonic jet mixing prompted several studies[5–11] to achieve enhanced mixing with the use of nonconventional nozzle geometries.

Lobed nozzles[7–11] consist of alternate crests and troughs and are found to enhance mixing over a wide range of flow parameters. Based on water flow visualization at very low speeds by Werle et al.[8] and measurements by Paterson[9] at subsonic speeds, the enhanced mixing performance was attributed to the generation of axial vortices. Unconfined flow experiments at supersonic speeds also showed evidence of mixing enhancement with use of lobed nozzles.[7] Narayanan and Damodaran[10] performed experiments with a radially lobed nozzle and reported enhanced mixing in confined flows relative to unconfined flow cases. They believed that the interaction of the divergent nozzle flow and the confining duct generated large-scale vortices, thus enhancing mixing. However, Werle et al.[8] and Tillman et al.[11] suggest that the formation of axial vortices is independent of the presence of an ejector shroud in rectangular-lobed nozzle flowfields. Another issue that merits attention is the assessment of mixing performance in light of the associated total pressure drops anticipated (a feature lacking in many previous investigations).

The freejet characteristics of lobed nozzles were recently investigated by Ramesh Kumar and Kurian.[12] The aim of the present investigation was to understand the factors affecting the jet dynamics of lobed nozzles in confined and unconfined coaxial flows, to document the enhanced mixing performance with the associated total pressure drop, and to assess the thrust losses resulting from the use of lobed nozzles. The other objectives were to study the effect of the confining duct on jet development, to examine the flowfield for the presence of vortices as also factors governing their generation at supersonic speeds, and to assess the effect of nozzle geometric parameters on the flowfield.

Experimental Facility and Test Procedure

The experiments were conducted in the two-stream coaxial blowdown facility used by Narayanan and Damodaran[10] (see Fig. 1a). The primary flow line was built such that suitably designed nozzles could be used interchangeably. All the primary nozzles were convergent-divergent, and the secondary flow line was fitted with a conical convergent nozzle. Air was the working medium for both streams and was supplied from a common reservoir, but the streams were controlled independently. A semiautomatic, three-dimensional traversing mechanism moved the pitot and cone-static probes axially and radially. A squarely faced tube with a 1-mm opening and 1.3-mm outer diameter formed the tip of the pitot probe. The cone-static probe was made based on the design of Kenworthy and Schetz[13] and consisted of a 10-deg semivertex angle cone of 1.7-mm base

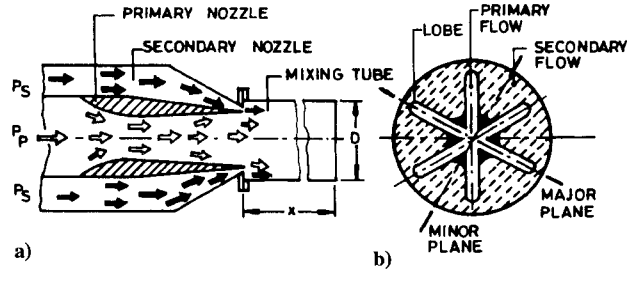

Fig. 1 Flow configuration: a) schematic of confined flow and b) end view of a six-lobed nozzle.

Received April 7, 1995; revision received Sept. 8, 1995; accepted for publication Oct. 2, 1995.

*Research Associate, Department of Aerospace Engineering.
†Associate Professor, Department of Aerospace Engineering.

diameter. Four holes of 0.35 mm (90 deg apart) were drilled perpendicular to the surface at about 3.7 mm from the vertex of the cone. The pitot and static probes produced area blockages of 0.26% and 0.44%, respectively, at the exit of the primary nozzles. The mean pitot and cone-static pressures were measured during different test runs. The pressures sensed were communicated to a transducer (accuracy ±0.5%) whose output was delivered to a calibrated digital interface unit. Cone flow tables and the Rayleigh pitot equation were used to obtain the local mean flow properties (e.g., total pressure, static pressure, Mach number). A schlieren system (from a steady light source) using two concave mirrors in an off-axis arrangement was used for flow visualization.

Jet axial thrust measurements were made in a separate facility that had provision only for primary flow. The facility consisted of a settling chamber suspended on four flexible leaf springs (to bear the weight), thus permitting free relative horizontal movement. Air supply to the settling chamber was perpendicular to the flow direction. During blowdowns, the settling chamber moved backward, bearing against a suitably positioned load cell (accuracy ±0.1%) whose analog output was converted to a digital display using an interfacing unit.

Four primary nozzles were used in this study. One was a conventional conical convergent-divergent nozzle with a semidivergence angle of 2.5 deg, whereas the others were radially lobed nozzles. All the nozzles, designed for $M_{ex} = 1.7$, had the same throat dimension and, hence, the same exit plane area. D_e (diameter of the circle with the same exit plane area) for all the nozzles was 25.5 mm. The lobed nozzles had a smooth circular cross-section convergence up to the throat, and the lobe contouring began downstream of the throat. The lobes had a constant width throughout, but their height varied from a minimum near the throat to a maximum at the exit plane. The end view of a six-lobed nozzle is shown in Fig. 1b. The lobed nozzles had radially arranged alternate troughs (formed between two adjacent lobes) and crests (formed by the lobes). The plane bisecting the width of the lobes is called the major plane, and the plane bisecting the troughs is called the minor plane (see Fig. 1b). A few geometric parameters of the nozzles are presented in Table 1. (See Ref. 14 for design drawings and photographs of the nozzles.) Nozzles E2 and S were designed to be similar in most possible aspects of design to enable the effect of the number of lobes on jet development to be understood. Nozzles E1 and E2 were used to study the effect of lobe height.

The secondary nozzles had a semiconvergence angle of 30 deg. The secondary nozzle used with nozzles C and E1 had an exit plane diameter of 42.2 mm, and the one used with nozzles S and E2 had an exit plane diameter of 48 mm (because of the larger lobe height of these nozzles).

The experimental test conditions (Table 2) are identified by a three-letter code. The letters U, C, D, and S denote unconfined, confined, dual, and single (primary) flows, respectively. The last numeral, ranging from 1 to 4, indicates the combination of reservoir stagnation pressures used. The pressure ratio for ideal expansion

Table 1 Nozzle geometric parameters and thrust measurements

Nozzle name	C	E1	E2	S
Description of the nozzle	Conical	Eight lobed	Eight lobed	Six lobed
Semidivergence angle, deg	2.5	——	——	——
Major plane	——	17	17	17
Minor plane	——	−12.6	−10.9	−10.3
Lobe height, mm	——	15.60	18.75	18.90
Exit plane perimeter, mm	80.1	261.5	305.4	243.2
$Re_\delta/10^5$ (at $x/D_e = 2.35$)	2.10	——	——	——
Major plane	——	——	7.24	7.77
Minor plane	——	——	3.46	3.93
T_m/T_c[a]	0.95	1.00	0.95	0.91
$T_m/(T_m)_{uc}$[a]	——	——	——	——
l/D[b] = 0.44	——	0.79	0.80	0.76
$l/D = 2.53$	0.57	0.60	0.39	0.41
$l/D = 4.44$	0.55	0.59	0.38	0.39

[a]Subscripts: m, measured; c, calculated; and uc, unconfined flow.
[b]l/D, length to diameter ratio of confining tube.

Table 2 Test conditions

Flow case	P_P, MPa	P_S, MPa	$(p_S/p_P)_{ex}$, MPa	$(\dot{m}_S/\dot{m}_P)$ C	S	E2	E1
UD1	0.59	0.23	1.00	0.71	1.16	1.10	0.71
CS1	0.59	——	——	——	——	——	——
CD1	0.59	0.23	1.00	0.71	1.16	1.10	0.71
CD2	0.59	0.18	1.00	0.53	0.89	0.84	0.54
CD3	0.50	0.23	1.19	0.84	1.38	1.31	0.85
CD4	0.50	0.18	1.00	0.67	1.10	1.04	0.67

of the primary nozzle was close to 5. Hence, $P_P = 0.50$ MPa and $P_P = 0.59$ MPa correspond to ideal and underexpanded (with respect to the ambient, 0.1 MPa) operation of the primary nozzles. Similarly, the secondary nozzle was operated either unchoked at $P_S = 0.18$ MPa or underexpanded at 0.23 MPa.

The uncertainties in estimating various quantities are: $P_P \pm 2\%$, $P_S \pm 1.5\%$, $\dot{m}_P \pm 2.2\%$, $\dot{m}_S \pm 1.7\%$ (these include errors resulting from variations during a run and from run to run), and $T \pm 1.0\%$. At $M = 1.5$ (a typical value), and with an assumed probe misalignment of 10 deg with the flow, the uncertainty in pitot pressure is ±2.9%. With an assumed uncertainty of ±10% in the cone-static pressure, the uncertainty in M is ±6.7% and in P is ±4.5%. The error associated with the estimation of δ is ±6.0%, of $d\delta/dx \pm 9.0\%$, of $\eta \pm 6.4\%$, and of $D_P \pm 9.3\%$.

Results and Discussion

A. Unconfined Coaxial Flow Studies

The radial total pressure profiles for nozzles C and E2 for case UD1 are shown in Fig. 2. The origin of the coordinate system is at the point of intersection of the nozzle exit plane and the jet axis. For the unconfined flows, the axial and radial coordinates are normalized by D_e and R_e, respectively. At the exit plane of nozzle C, the primary flow is limited to $r/Re = 1$, and the secondary flow ranges from $r/R_e = 1$ to 1.65. The profiles show the gradual spread of the jet with increasing axial distance. However, even at the last axial location, the total pressure is high in the central region and low in the outer region, indicating a slow rate of transfer of momentum. For the lobed nozzles, measurements were made along the major and minor planes. At the exit plane of nozzle E2, the primary flow issues through the central region and the lobes, i.e., up to $r/R_e = 1.76$ along the major plane; the secondary flow issues beyond $r/R_e = 0.73$ in the minor plane. The nonuniform profile and the large jet spread along the major plane are characteristics of the lobed nozzle flowfield.[12] At $x/D_e = 1.57$, the Mach numbers observed along the minor plane indicated a central high-speed region, a low-speed outer region and, finally, the spreading of the jet into the ambient atmosphere at the edge of the profile. The profiles at downstream locations indicate the rapid spreading of the jet along both planes and the reduction of differences in total pressure between the planes. However, the profiles exhibit radial nonuniformity. The values of

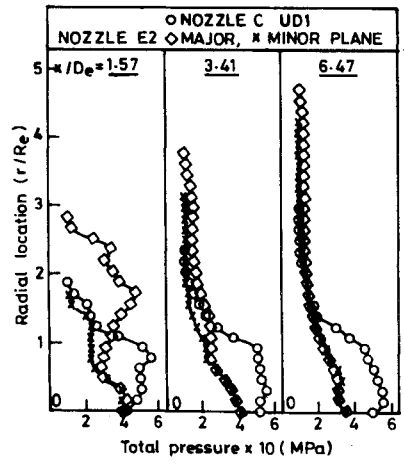

Fig. 2 Radial total pressure profiles for nozzles C and E2 (unconfined flow).

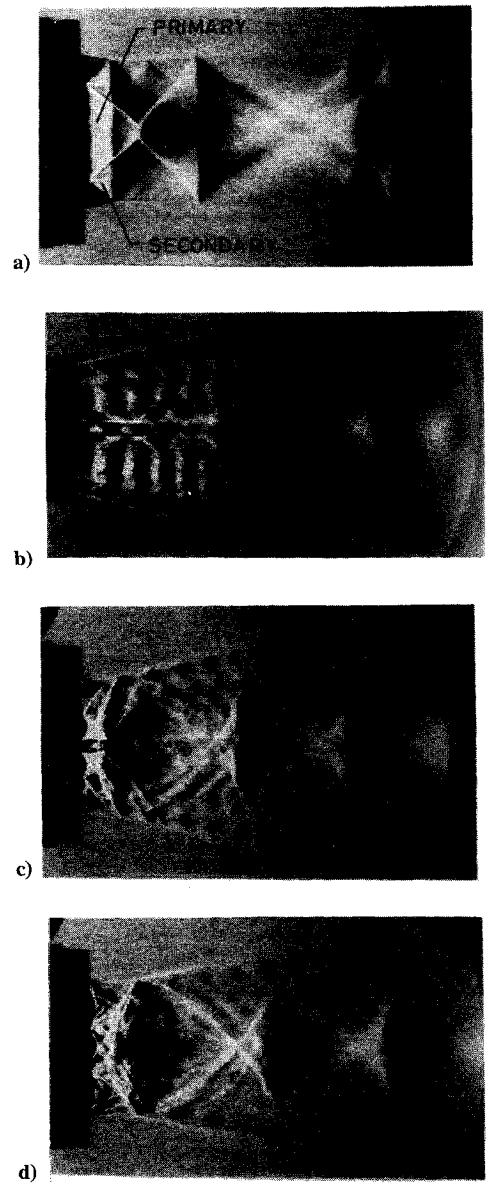

Fig. 3 Schlieren photographs of unconfined flows (flow from left to right): a) dual jet from nozzle C, b) single freejet from nozzle E1 (major plane), c) dual jet from nozzle E1 (major plane), and d) dual jet from nozzle E1 (minor plane).

total pressure in the jet are lower than the corresponding values for the conical nozzle. A similar trend of pressure decay was observed in the freejets from lobed nozzles.[12] Hence, the presence of the outer flow did not alter this characteristic behavior of the lobed nozzles. The profiles for nozzle S also exhibited a similar trend. The centerline pitot pressure was seen to decay rapidly, reaffirming the large spreading of the jets.

Figure 3a is the schlieren photograph (knife-edge orientation vertical) of case UD1 for nozzle C. The shocks in the central region are because of the underexpanded operation of the primary and secondary nozzles. Near the nozzle exit, a strong compression (bright) region is seen, contrary to expectation in an underexpanded flowfield. This apparent anomaly is because of the presence of secondary flow, which confines the inner flow. An expansion (dark) region is seen downstream of the crossing point of the intercepting shocks. The internal system of shocks observed in conical nozzle flow is also seen. The second shock cell is longer than the first, and the cell lengths of both systems of shocks appear to be the same.

Figures 3b–3d are schlieren photographs for nozzle E1 (which subsequently will be used for comparison with the confined flow photographs). Figures 3b and 3c are photographs (obtained when the major plane is oriented perpendicular to the light direction) of the primary and dual flows, respectively. As noted in Ref. 12, the freejet (Fig. 3b) gives rise to alternate expansion-compression regions. However, because of the presence of the confining secondary flow, the flow from the lobed nozzle is compressed (bright) near the exit and a curved Mach disk is formed as for nozzle C. Further downstream, an intense expansion (dark) region is seen. The short horizontal shock structure close to the nozzle exit along the jet axis is due to projection of the image of the flow from horizontally oriented lobes.[12] Also note the large spread of the jet (see Figs. 3a and 3c). In Fig. 3d (view of the jet along the minor plane), the jet spread is observed to be lower, and the second shock cell longer, than in the major plane.

To quantify the observations on jet spread, the shear-layer thicknesses were calculated. Because of the large decay of total pressure, local values are used to define δ (e.g., Refs. 6 and 12). To estimate the thickness of the shear layer generated as a result of the interaction of the primary and secondary flows, the suggestion by Dufflocq et al.[16] to obtain the edge of the shear layer was used. Shear-layer thickness δ was defined as the difference between radial locations, where P assumed values of $P_{edge} + k(P_{cl} - P_{edge})$ and $P_{edge} + (1-k)(P_{cl} - P_{edge})$ (because the flow was unconfined, P_{edge} corresponds to the ambient pressure). A value of 0.0675 for k was found to fit the present measurements with nozzle C to the planar shear-layer data in Ref. 2; hence, this value of k was used for all nozzles. From Fig. 4, δ for the lobed nozzle is observed to be considerably higher than that for nozzle C.

The Reynolds number based on $\delta - Re_\delta$ (at $x/D_e = 2.35$) for the nozzles is listed in Table 1. These values exceed 2×10^5, satisfying the criterion of Ref. 3 (modified to account for the definition of δ used here) for fully developed flow. However, the profiles were found to be reasonably self-similar only from $x/D_e = 3.41$ and, hence, these profiles were used to determine the growth rate. Figure 5 shows the

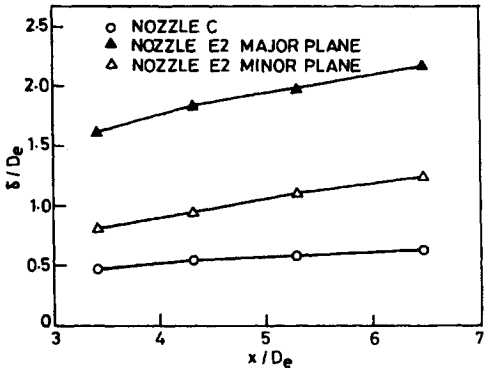

Fig. 4 Shear-layer thicknesses for nozzles C and E2.

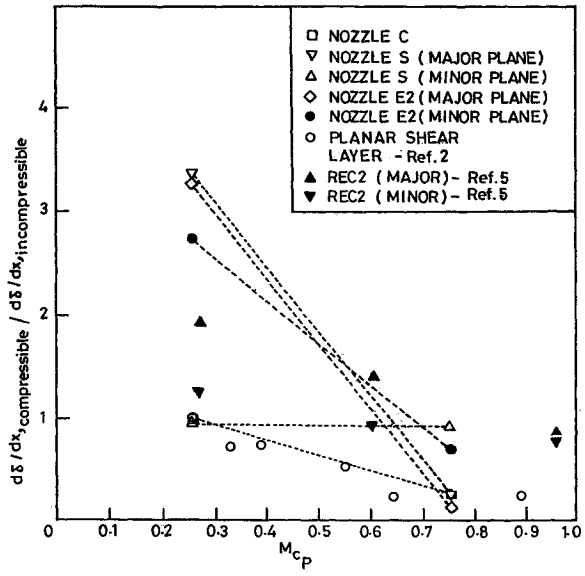

Fig. 5 Normalized shear-layer growth rate for the nozzles.

growth rate data for planar shear layers from Ref. 2, coaxial jets from Ref. 5, and the freejet at $M_c = 0.75$ (see Refs. 2 and 15 for definition of M_c) from Ref. 12, along with the data for case UD1 (at $M_c = 0.26$). Because of the lack of known incompressible shear-layer growth rate data for lobed nozzles, the growth rate data for all the nozzles were normalized by the expression given in Ref. 2, i.e.,

$$\frac{d\delta}{dx} = 0.14(1-r)\frac{1+s^{\frac{1}{2}}}{1+rs^{\frac{1}{2}}}$$

where $r = u_S/u_P$ and $s = \rho_S/\rho_P$. The normalized growth rates are plotted against M_c, and the data for the lobed nozzles are connected to show their relative positions. Figure 5 gives a relative estimate of the spreading rate of various nozzles. Considerable increase in the normalized growth rate is observed for the lobed nozzles. The average growth rate for nozzle E2 is higher than that of nozzle S. The growth rate is higher in the major plane than in the minor plane, contrary to the trend observed from the freejet study (of primary flow). The secondary flow was shown to confine the primary flow and, as a considerable portion of the secondary flow surrounds the primary flow in the minor plane, the high spreading rate of the freejet along this plane is reduced. On the contrary, the extent of secondary flow enclosing the primary flow in the major plane is less and, hence, the growth rate is rather enhanced because of the outward radial velocity component of the flow from the lobes and the underexpanded operation of the primary nozzle. This could explain the differences between the single freejet and coaxial flow cases.

B. Effect of Confining Duct on the Development of Primary Flow

The radial pressure profiles for case CS1 for nozzle S are shown in Fig. 6. Schlieren images revealed considerable interaction of the flow with the mixing tube wall. Hence, the axial and radial coordinates are normalized by the mixing tube diameter D and radius R. Radial measurements were made at the exit plane of mixing tubes of five lengths ($x/D = 0.44$–4.44). At $x/D = 0.44$, the flow along the minor plane is confined to the initial central region. The profile along the major plane is distorted from interaction with the mixing tube wall. The profiles at $x/D = 0.76$ show a transfer of momentum between the planes. By $x/D = 1.64$, there is equalization of pressures, and the profiles at further downstream locations indicate a mixed but highly dissipated subsonic flow. Profiles for nozzle C also show effects of dissipation (a portion of the flow becomes subsonic), but the profiles are nonuniform in the radial direction, indicating a poor tendency for transport of properties.

To assess the extent of dissipation, thrust measurements were made. Study of freejets[12] showed that the observed primary flow thrust loss could be attributed to loss in axial momentum because of divergent nozzle flow (see T_m/T_c in Table 1). The thrust values for mixing tubes of different lengths are also presented in Table 1. Thrust losses for nozzles C and E1 are lower than those for nozzles E2 and S because the mixing tube cross-sectional area for the latter pair of nozzles is 1.37 times that of nozzles C and E1 (indicating the possibility of higher duct frictional losses).

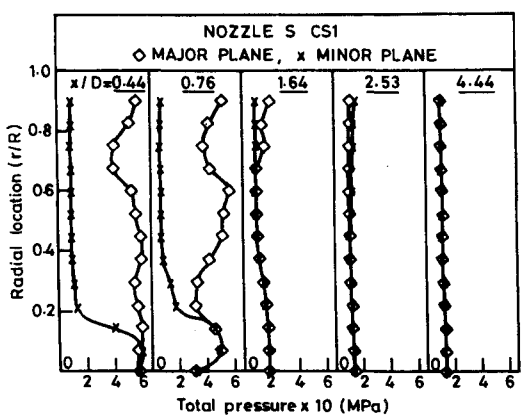

Fig. 6 Radial total pressure profiles for nozzle S (confined single flow).

C. Confined Flow Studies

The profiles for nozzles C and E1 for case CD1 are shown in Fig. 7. The flows were supersonic at all axial locations. The profiles for nozzle C show a slow rate of radial transport of properties. Even at the last axial location, considerable nonuniformity of total pressure is observed. At $x/D = 0.44$, the Mach numbers along the minor plane of nozzle E1 indicate a high-speed central region and a low-speed outer one. This difference diminishes at axial locations downstream. The reduction in pressures along the major plane and the simultaneous increase in the minor plane indicate considerable transport between the planes, resulting in reasonably uniform profiles along both planes at $x/D = 4.44$. Plots for other confined flow cases also show trends similar to CD1. The relative magnitudes of the profiles are in conformity with the magnitude of upstream pressure settings.

The schlieren photographs of the foregoing cases are shown in Fig. 8. The use of a mixing tube compresses the flow (see Fig. 3) to a

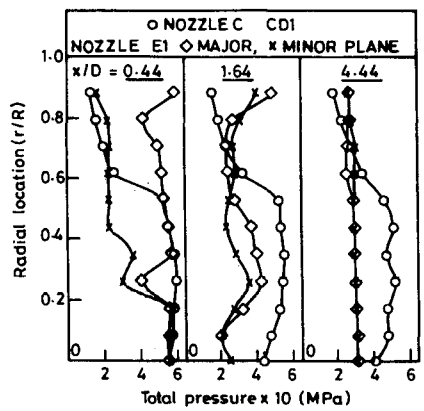

Fig. 7 Radial total pressure profiles for nozzles C and E1 (confined dual flow).

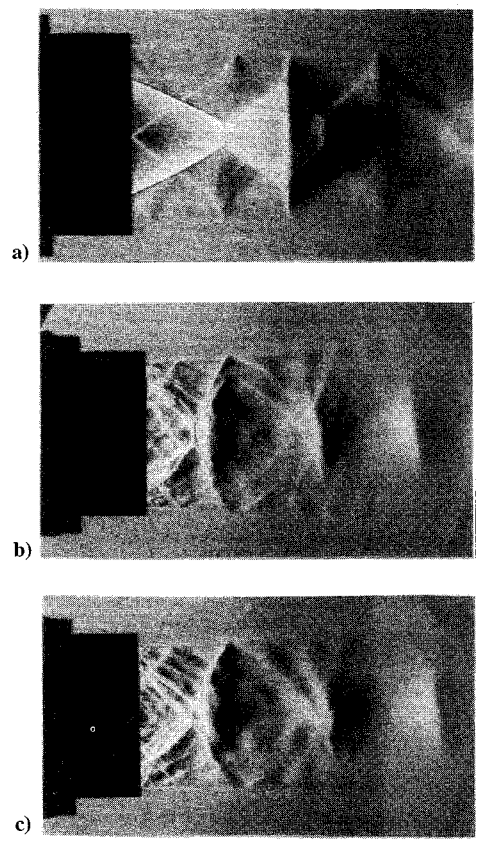

Fig. 8 Schlieren photographs of confined jets (mixing tube of x/D = 0.44): a) from nozzle C, b) from nozzle E1 (major plane), and c) from nozzle E1 (minor plane).

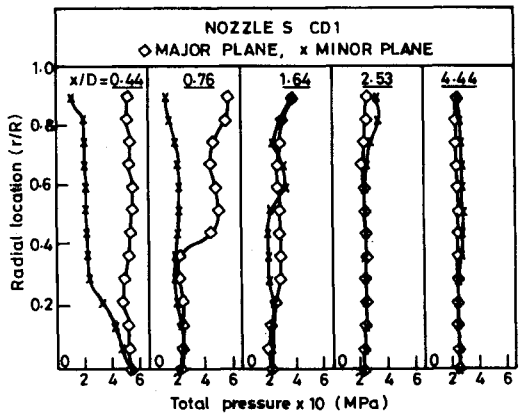

Fig. 9 Radial total pressure profiles for nozzle S (confined flow).

greater extent than the unconfined cases (as evident from the bright regions and elongated shock cells), thus forcing the interaction of the primary and secondary flows. This is the reason for the increased radial uniformity of the confined flow profiles. Further, the use of a mixing tube is found to reduce the divergent nature of the flow from nozzle E1 (see Figs. 3c and 3d).

The profiles for nozzle S for case CD1 are shown in Fig. 9. At $x/D = 0.44$, the profile along the major plane is nearly uniform; in the minor plane, however, three distinctive regions are seen: a central high-pressure region, followed by a uniform region of low pressure (resulting from the secondary flow) and an outer region where no flow takes place. The distortion of the profile along the major plane at $x/D = 0.76$ is because of the interaction of the jet with the duct. The profiles at $x/D = 1.64$ show the transport of momentum across the planes. Comparison with Fig. 6 shows the effect of the presence of the secondary flow on the development of primary flow. By $x/D = 4.44$, the profiles along the major and minor planes are almost uniform. However, some differences exist, indicating the possibility for further mixing. Also, these profiles reveal a mean value greater than the P_S value. Considering the dissipation associated with mixing, this provides evidence of transport of momentum across the planes. The profiles for nozzle E2 show increased uniformity but are associated with a further drop in the mean value of total pressure.

Mixing Performance Evaluation

Although decay of centerline properties, shear-layer growth rates, and uniformity of mean flow profiles are used to assess mixing, they are not definitive indicators of molecular-scale mixing essential for combustion. The problem is further compounded in the mixing of two streams using air as the working medium (with the same inlet total temperature and without additives to mark the flow) because stream identification is difficult. However, gas sampling measurements of Gutmark et al.[6] suggest that pressure measurements could be used to make reasonable estimates of initial stages of mixing. Ramesh Kumar and Kurian[17] showed that total pressure is the more appropriate physical quantity to amplify the existing nonuniformity and to check for mixing. They developed a mixing parameter (η) to assess the extent of mixing in a given flow cross section; an outline of the formulation follows.

Measure of the radial nonuniformity of total pressure (K_r) was obtained by

$$K_r^2 = \frac{1}{R}\int_0^R [E_P(r)]^2\,dr$$

where $E_P(r) = [P(r) - P_m]/P_m$ if $M(r) \geq M_m$ or vice versa; m denotes the mean value along the radial direction.

Because of the difference in inlet conditions along the major and minor planes for the lobed nozzles, an additional check for uniformity between the planes was made by K_P, where

$$K_P^2 = \frac{1}{\pi R^2}\int_0^R [E_P(r)]^2 2\pi r\,dr$$

where $E_P(r) = [P(r)_{\text{major}} - P(r)_{\text{minor}}]/P(r)_{\text{minor}}$ if $M(r)_{\text{major}} \geq M(r)_{\text{minor}}$ or vice versa. Thus, $\eta = K_r$ for the conical nozzle, and $\eta = [0.5(K_{r_{\text{major}}} + K_{r_{\text{minor}}}) + K_P]/2$ for lobed nozzles, and the lower the value of η, the better the mixing of the flows.

Figure 10 shows the mixing performance of the nozzles tested. As also observed from the pressure profiles, nozzle C shows the least efficient mixing performance. Although nozzles S and E1 exhibit similar values of η, the performance of nozzle S can be considered better, since a large mass of secondary flow has been mixed (see Table 2). Nozzle E2 has a lower value of η than that of nozzles S and E1. The values of η for lobed nozzles indicate that both increasing the number of lobes from six to eight and increasing the lobe height provide some additional mixing enhancement.

Total Pressure Drop Parameter

Large total pressure drops were observed as a results of the mixing process, especially at locations farther downstream. To estimate these losses, the total pressure drop parameter of Fuller et al.[18] was adapted to the present flow conditions. D_P is defined as the ratio of the mass–weighted total pressure at any cross section to the sum of inlet mass–weighted total pressures of the two flows (the lower the D_P value, the larger the drop in total pressure).

Figure 11 shows the value of D_P for the nozzles. The conclusions from this plot are similar to those from Fig. 10. The pressure drop is maximum for nozzle E2 and least for nozzle C, and the pressure drops for nozzles S and E1 are similar. The correspondence between the mixing performance and the pressure drop is anticipated, because mixing is inevitably associated with some pressure drop. Similar trends were also observed from the total pressure profiles.

D. Laser Light Sheet Visualization

Laser light sheets (LLS) have been used to obtain qualitative pictures of jet flowfields (e.g., Naughton et al.[19] and Zaman et al.[20]). In the present work, an LLS formed from a 10-mW He-Ne cw laser beam was used to make cross-sectional (perpendicular to jet axis) cuts of the flow. Artificial seeding was found essential; hence, water droplets were injected perpendicular to the flow direction into

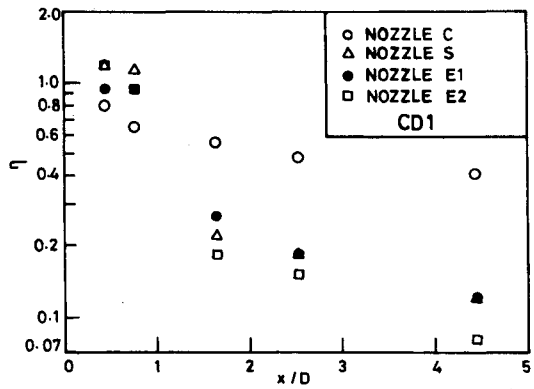

Fig. 10 Variation in the mixing parameter for the nozzles.

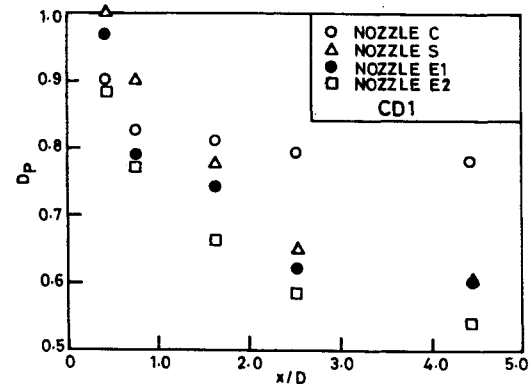

Fig. 11 Variation in total pressure drop factor for the nozzles.

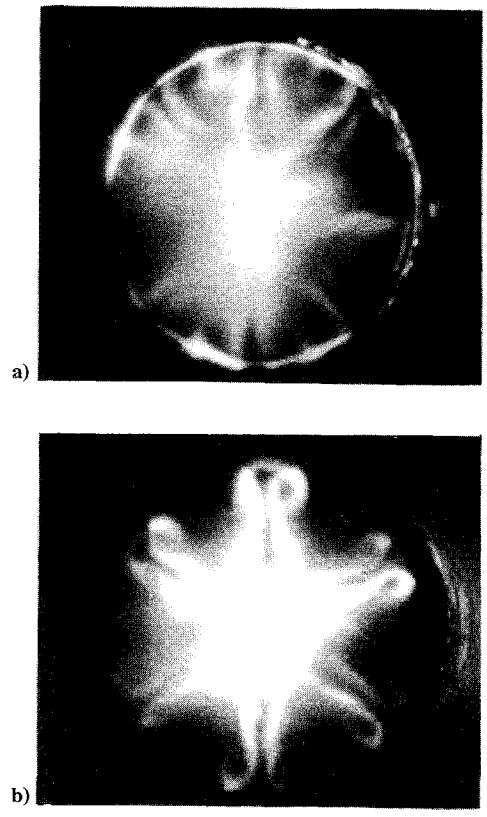

Fig. 12 LLS illuminated cross section at: a) x/D = 0.76 (nozzle E2) and b) x/D_e = 0.90 (nozzle S).

the secondary settling chamber. The expected ringlike pattern with the conical primary nozzle was obtained. Figure 12a shows an LLS photograph of the confined jet (case CD1). The turning of the flow at the tips of the lobes and the interactions of the flows from adjacent lobes with the mixing tube wall are evident. The primary flow is observed to entrain the particles, effectively marking the interface between the primary and secondary flows. The LLS photograph of the unconfined jet (case UD1) in Fig. 12b reveals marked turning of the flow (formation of vortices) near the tips of the lobes. Cuts of the flowfield with the LLS tilted at various angles confirmed the axial nature of the vortices. These photographs also suggest that the vortices cause the transport of primary flow to the minor plane. Because of the blowdown nature of the facility, the photographs were taken at an angle, and exposure time of several seconds was found essential. This is the reason for superposition in the central portions of the photographs. The structures were, however, visually steady and clear.

Detailed cross-sectional probe surveys made for cases CD1 and UD1 with nozzle E2 (the resulting Mach number contours are shown in Figs. 13a and 13b) confirmed the ability of the particles to track the flow and also the presence of vortices. As seen from the LLS photographs, the flow in Fig. 13a is observed to turn at the tips of the lobes that is, to form vortex structures, and interact with the mixing tube wall and adjacent lobes. Figure 13b shows the contours of the flow at a location farther downstream; although the jet spread is large, the turning of the flow near the edges of the lobes remains clear, and the pattern visualized also confirms this observation.

These preliminary results clearly show that axial vortices are generated in unconfined and confined flows from radially lobed nozzles. Similar results have been observed at lower speeds.[8,9,21] The axial vorticity observed could be generated as a result of cross-stream shear and turning of the upstream boundary layer (Waitz et al.[22]). However, in the work of McCormick and Bennett[21] (at low speeds) and Elliott et al.,[23] the boundary layer was not primarily responsible for the observed vorticity. The oppositely directed radial velocity components of the primary and secondary flows (especially at the lobe tips) generate considerable cross-stream shear and, hence, could be responsible for the generation of vortices.

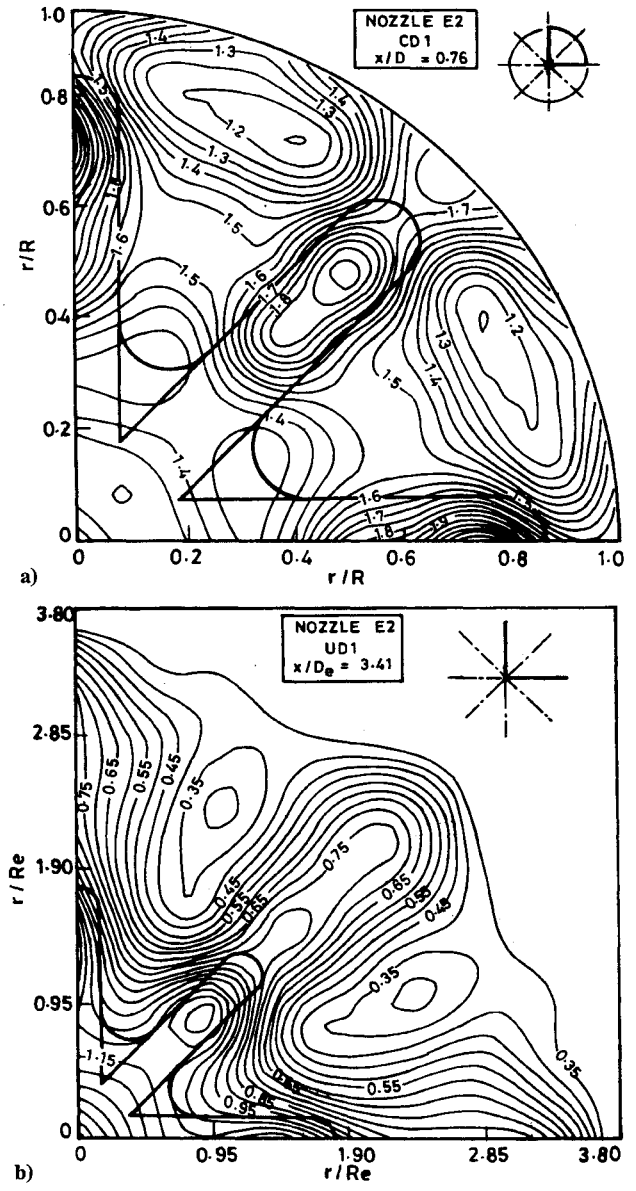

Fig. 13 Mach number contours (data reflected about axis of symmetry): a) confined flow at x/D = 0.76 and b) unconfined flow at x/D_e = 3.41.

Conclusions

The freejet studies of lobed nozzles revealed that thrust loss was due primarily to divergent nozzle flow. The numerous weak shocks in the flowfield, increases in the number of lobes, and wetted surface area had only a secondary effect. Use of a confining duct was found to reduce thrust primarily because of friction losses.

Alternate expansion-compression regions (from the lobes) characterized the freejets from lobed nozzles. However, the presence of secondary flow was found to confine the primary flow and generate stronger compression-expansion regions. Increases in the number of lobes and lobe height were not found to alter the jet pattern significantly. LLS visualization revealed the presence of axial vortices in both unconfined and confined flows from radially lobed nozzles. The vortices caused transport of primary flow to the minor plane and appeared to be formed as a result of cross-stream shear.

The spreading rate of the unconfined flows from lobed nozzles was more than twice that from the conical nozzle. The pressure profiles show increased radial uniformity and transport of properties between the planes. Use of a mixing tube was found to force the interaction of primary and secondary flows and enhance mixing. The η value of a lobed nozzle was a fifth of the value for the conical nozzle, indicating significant improvement in mixing performance. Increases in the number of lobes (from six to eight) and in the lobe

height also produced additional mixing. The pressure drop for the lobed nozzles was considerably higher (for nozzle E2, it was ca. 1.5 times higher) than that of the conical nozzle.

This study also shows that an increase in the number of lobes and in lobe height, with divergence angle unaltered, results in enhanced mixing performance but causes larger drops in total pressure. Reduction in nozzle divergence angle would reduce thrust loss and improve the pressure drop characteristics but would be associated with loss in mixing performance.

Acknowledgments

The authors are grateful to G. A. Venceslas, Technical Officer, and S. Manoharan, Project Technician, for their valuable suggestions and deep involvement in the experiments. Thanks are due to T. V. Ramana Rao, undergraduate student, for his help with the schlieren system and to C. Wilbert, K. Balasundaram, M. Karuppiah, and K. Lakshmi.

References

[1]Chinzei, N., Masuya, G., Komuro, T., Murakami, A., and Kudou, K., "Spreading of Two-Stream Supersonic Turbulent Mixing Layers," *Physics of Fluids*, Vol. 29, No. 5, 1986, pp. 1345–1347.

[2]Papamoschou, D., and Roshko, A., "The Compressible Turbulent Shear Layer: An Experimental Study," *Journal of Fluid Mechanics*, Vol. 197, 1988, pp. 453–477.

[3]Goebel, S. G., and Dutton, J. C., "Experimental Study of Compressible Turbulent Mixing Layers," *AIAA Journal*, Vol. 29 , No. 4, 1991, pp. 538–546.

[4]Clemens, N. T., and Mungal, M. G., "Two- and Three-Dimensional Effects in the Supersonic Mixing Layer," *AIAA Journal*, Vol. 30, No. 4, 1992, pp. 973–981.

[5]Schadow, K. C., Gutmark, E., and Wilson, K. J., "Compressible Spreading Rates of Supersonic Coaxial Jets," *Experiments in Fluids*, Vol. 10, 1990, pp. 161–167.

[6]Gutmark, E., Schadow, K. C., and Wilson, K. J., "Effect of Convective Mach Number on Mixing of Coaxial Circular and Rectangular Jets," *Physics of Fluids A*, Vol. 3, No. 1, 1991, pp. 29–35.

[7]Tillman, T. G., Patrick, W. P., and Paterson, R. W., "Enhanced Mixing of Supersonic Jets," AIAA Paper 88-3002, July 1988.

[8]Werle, M. J., Paterson, R. W., and Presz, W. M., Jr., "Flow Structure in a Periodic Axial Vortex Array," AIAA Paper 87-0610, Jan. 1987.

[9]Paterson, R. W., "Turbofan Mixer Nozzle Flow Field—A Benchmark Experimental Study," *Journal of Engineering for Gas Turbines and Power*, Vol. 106, 1984, pp. 692–698.

[10]Narayanan, A. K., and Damodaran, K. A., "Experimental Studies on Mixing of Two Co-Axial High-Speed Streams," *Journal of Propulsion and Power*, Vol. 10, No. 1, 1994, pp. 62–68.

[11]Tillman, T. G., Paterson, R. W., and Presz, W. M., Jr., "Supersonic Nozzle Mixer Ejector," *Journal of Propulsion and Power*, Vol. 8, No. 2, 1992, pp. 513–519.

[12]Ramesh Kumar, R., and Kurian, J., "Studies on Freejets from Radially Lobed Nozzles," *Experiments in Fluids*, Vol. 19, 1995, pp. 95–102.

[13]Kenworthy, M., and Schetz, J. A., "An Experimental Study of Slot Injection into a Supersonic Stream," NASA CR-2128, Jan. 1973.

[14]Ramesh Kumar, R., "Studies on Mixing of Two High Speed Streams," B.Tech. Thesis, Dept. of Aerospace Engineering, Indian Inst. of Technology, Madras, India, 1994.

[15]Bogdanoff, D. W., "Compressibility Effects in Turbulent Shear Layers," *AIAA Journal*, Vol. 21, No. 6, 1983, pp. 926, 927.

[16]Dufflocq, M., Benjamin, M. A., Roan, V. P., and Lear, W. E., "Initial Development of the Axisymmetric Ejector Shear Layer," AIAA Paper 92-3567, July 1992.

[17]Ramesh Kumar, R., and Kurian, J., "Estimation of Mixing of High-Speed Streams," *Journal of Propulsion and Power* (to be published).

[18]Fuller, E. J., Mays, R. B., Thomas, R. H., and Schetz, J. A., "Mixing Studies of Helium in Air at High Supersonic Speeds," *AIAA Journal*, Vol. 30, No. 9, 1992, pp. 2234–2243.

[19]Naughton, J., Cattafesta, L., and Settles, G., "An Experimental Study of the Effect of Streamwise Vorticity on Supersonic Mixing Enhancement," AIAA Paper 89-2456, July 1989.

[20]Zaman, K. B. M. Q., Reeder, M. F., and Samimy, M., "Control of an Axisymmetric Jet Using Vortex Generators," *Physics of Fluids*, Vol. 6, No. 2, 1994, pp. 778–793.

[21]McCormick, D. C., and Bennett, J. C., Jr., "Vortical and Turbulent Structure of a Lobed Mixer Free Shear Layer," *AIAA Journal*, Vol. 32, No. 9, 1994, pp. 1852–1859.

[22]Waitz, I. A., Marble, F. E., and Zukoski, E. E., "Vorticity Generation by Contoured Wall Injectors," AIAA Paper 92-3550, July 1992.

[23]Elliott, J. K., Manning, T. A., Qiu, Y. J., Greitzer, E. M., Tan, C. S., and Tillman, T. G., "Computational and Experimental Studies of Flow in Multi-Lobed Forced Mixers," AIAA Paper 92-3568, July 1992.